Investigating the influence of acid sites in continuous methane oxidation with N_2O over Fe/MFI zeolites

Ying Kit Chow[a], Nicholas F. Dummer[a]*, James Carter[a], Christopher Williams[a], Greg Shaw[a], David J. Willock[a], Stuart H. Taylor[a], Sara Yacob[b], Randall J. Meyer[b], Madan M. Bhasin[c] and Graham J. Hutchings[a]*

[a] Cardiff Catalysis Institute, School of chemistry, Cardiff University, Cardiff CF10 3AT, UK.

[b] ExxonMobil Research and Engineering Company, Corporate Strategic Research, Annandale, NJ 08801, USA

[c] Innovative Catalytic Solutions, LLC, Charleston, WV, 25314, USA.

* Corresponding author email: dummernf@cardiff.ac.uk and hutch@cardiff.ac.uk

Abstract

Methane oxidation using N_2O was carried out with Fe-MFI zeolite catalysts at 300 °C. Methane conversion over Fe-ZSM-5, Fe-silicalite-1 and Fe-TS-1 indicates that Brønsted acidity is required to support the Fe-based alpha-oxygen active site for the important initial hydrogen abstraction step. Increasing the calcination temperature of Fe-ZSM-5 from 550 to 950 °C showed that the catalyst retained the MFI structure. However, at 950 °C the Brønsted and Lewis acid sites were altered significantly due to the migration of aluminium, which led to a significant decrease in catalytic performance. Over Fe-ZSM-5 the desired partial oxidation product, methanol was observed to undergo a reaction path similar to the methanol to olefin (MTO) process, which predominately produced ethene and subsequently produced coke. Methanol control experiments over Fe-silicalite-1, Fe-ZSM-5, Fe-TS-1 and H-ZSM-5 indicated that with the presence of Brønsted acidity the catalyst were more effective at forming ethene and subsequent aromatic species from DME, which resulted in an increased level of catalyst fouling. The implication of these observations are that the desorption of methanol is crucial to afford high mass balances and selectivity, however, Brønsted acid sites appear to slow this rate. These sites appear to effectively retain methanol and DME under reaction conditions, leading to low mass balances being observed. Our results confirm that to afford efficient and continuous methane oxidation by N_2O, the catalytic active site must be extra-framework Fe coordinated to Al.

Keywords; methane oxidation, methanol, N_2O, continuous reaction, Brønsted acidity.

Introduction

Methane is the major component of natural gas and the precursor to many valuable hydrocarbon products, including methanol.[1] However, it is under-utilised as a direct chemical feedstock and is currently converted to synthesis gas (CO and H_2) using high temperatures and pressures prior to the production of more valuable platform chemicals. Although selective, the current industrial syngas production process is highly energy-intensive.[2] Therefore a process for the direct partial oxidation of methane to methanol is highly desirable.[3]

However, the direct selective oxidation of methane to methanol is considered one of the most challenging reactions.[4] The central issue concerns the strong C-H bonds in methane, which have a bond dissociation energy of 438.8 kJ mol^{-1} and partial oxidation products typically have one or more C-H bonds weaker than this.[5, 6] The implication is that potential products are more reactive than methane and, therefore, over-oxidation to CO_2 is common.[7]

Panov and co-workers reported that methane could be activated over Fe-ZSM-5 by α-oxygen species when using N_2O as the oxidant.[8, 9] The α-oxygen was generated by decomposing N_2O over the reversible redox α-Fe sites, which switch from Fe^{2+} to Fe^{3+} (equation 1).[10] The radical anionic nature of the α-oxygen species allows the cleavage of the methane C-H bond *via* the hydrogen abstraction mechanism to occur at room temperature.[11]

$$N_2O + (Fe^{2+})_\alpha \rightarrow (Fe^{3+} - O^{\cdot-})_\alpha + N_2 \qquad (1)$$

The methoxy and hydroxyl groups formed are subsequently adsorbed on the α-Fe sites, which can yield methanol directly on the surface of the zeolite. At low temperatures, this process is quasi-catalytic as methanol must be extracted from the catalyst surface *via* hydrolysis.[10] However, above 300 °C methanol desorbs and the process is catalytic.[12]

The structure of the active site is, however, still debatable and is considered to comprise of either mono-nuclear Fe^{4+}=O (or Fe^{3+}-O^{-}) or di-nuclear Fe as an oxo-bridged $Fe^{3+}O^{2-}Fe^{3+}$ species[13]. Synder *et al.*[14] recently reported mononuclear α-Fe^{2+} in an extra-lattice site within Fe-beta zeolite (BEA) from magnetic circular dichroism spectroscopy. The reactive intermediate in this case was described as a high spin Fe^{4+}=O species, whereby the confinement of the zeolite lattice facilitates the reactivity observed. Hutchings and co-

workers reported di-nuclear Fe sites in Fe-ZSM-5, derived from EXAFS measurements and these were considered the active site for methane oxidation by H_2O_2 [15, 16]. Conversely, Dubkov *et al.*[17] reported on the formation of the active oxygen species upon decomposition of N_2O in Fe-ZSM-5 with Mössbauer spectroscopy. Adjacent Fe^{2+} atoms behaved as mono-nuclear sites when transformed to Fe^{4+}=O.

Analysis of the methane oxidation products by N_2O over Fe-ZSM-5 indicated that carbon oxides were the main product produced and oxygenates such as methanol, dimethyl ether (DME), acetaldehyde and higher hydrocarbons such as ethane were also produced.[10, 12] Catalyst fouling in the form of coke deposits were also observed in post reaction samples.[12, 18] Under low reaction temperatures (<300°C), after the formation of methanol from the recombination of methoxy and hydroxyl species, DME was extracted. This secondary product was considered to form as a result of a prolonged residence time of methanol on the surface of Fe-ZSM-5.[12] However under the catalytic regime at higher temperatures reported from the same group, DME was not detected in the gas-phase and was proposed to be the precursor to catalyst fouling. Therefore, methanol can either desorb directly from Fe-ZSM-5 or accumulate on the zeolite surface depending on the operating temperature.[12] It was reported that the activation energy of the surface diffusion of adsorbed species is much lower than the activation energy of desorption, implying that it is more favourable for the adsorbed methanol to diffuse across to other acid sites on the zeolite and carry out further reactions to form coke.[12, 19]

Copper and iron containing zeolites are known to be effective catalysts for methane oxidation.[15, 20, 21] The zeolite structure has a high adsorption potential within its porous environment, which gives rise to a confinement effect and in effect weakens the strong C-H bond in methane.[22] The Brønsted and Lewis acid sites both play a role in this reaction. Narsimhan *et al.* reported that the presence of Brønsted acid sites results in higher specific activity and space-time-yield (STY) for the Cu-containing zeolite with different topology such as ZSM-5 and mordenite. Furthermore, the apparent activation energy in the case of the protonated form of Cu-ZSM-5 was calculated to be approximately 30 kJ mol^{-1} higher from its Na analogue.[20] The Lewis acid sites are formed in the zeolite framework by exchanging with a metal precursor or through dealumination.[23] This allows metal ions to incorporate into the framework and/or extra framework positions. The extra-framework Lewis acid species can

increase the acid strength and the catalytic activity of zeolites due to an interaction with the Brønsted Si(OH)Al site.[24, 25] It was reported that Lewis acid sites were required for the hydroxylation of benzene with N_2O yielding 70-80% phenol with high selectivity and regioselectivity.[26] The two types of acid sites in the zeolite catalyse a wide range of chemical reactions from alkylation and isomerisation of hydrocarbons, cracking and hydrocracking processes, which are currently used in industry.[23]

In the present work, we have investigated continuous methane oxidation over Fe exchanged MFI framework zeolites with various acidity profiles using N_2O as a mild oxidant. Here we confirm that the combination of Fe and Al are required to activate methane. However, the presence of Al also provides a competing reaction path comparable to the methanol-to-olefin (MTO) type reaction mechanism, that is converting methanol to ethene and active aromatic intermediates in zeolites. We report the importance of acidity for the activation of methane, demonstrated by calcining a series of MFI-based zeolites at different temperatures. Furthermore, methanol control experiments and temperature programmed desorption experiments were carried out to understand the complex reaction mechanism present in the continuous, direct oxidation of methane by N_2O.

Experimental

Preparation of H-ZSM-5

The commercially available zeolite materials used in this study were activated by converting to the acidic protonated form prior to use by high temperature calcination. An example using ZSM-5 is listed as follows.

NH_4-ZSM-5 (Zeolyst, SiO_2:Al_2O_3 molar ratio = 30, 3 g) was transferred into a ceramic combustion boat and placed inside a quartz tube within a combustion furnace. The glass tube was then sealed and air was flowed through the catalyst. The furnace was heated to the desired temperature (typically 550 °C at 20 °C min^{-1}) and held for the required period of time (typically 3 h). The sample was allowed to cool to room temperature under flowing air prior to any testing or other modifications such as ion exchange with a metal precursor.

A series of catalysts were then prepared using the ion-exchange procedure are listed in the following section. A commercial zeolite material was exchanged once with the desired metal precursor using different synthetic approaches.

Commercially available TS-1 (Si:Ti = 25) from ACS Material was used in this study.

Preparation of Fe-ZSM-5

H-ZSM-5 (Zeolyst, SiO_2:Al_2O_3 molar ratio = 23-280) was used to prepare all the catalysts prepared by chemical vapour infiltration (CVI) unless stated otherwise. The full procedure for the CVI procedure for 2 wt. % Fe/ZSM-5 (30) is outlined as follows. The desired amount of H-ZSM-5 (1.98 g) and Fe (III) acetylacetonate ($Fe(acac)_3$) (Sigma Aldrich, 99.9% purity, 2.53 g) were added to a Schlenk flask. The metal precursor and zeolite were mixed well and heated to sublimation deposition temperature (150 °C) under continuous vacuum (*ca* 10^{-3} mbar) for typically 2 h. The catalyst was then allowed to cool to room temperature before calcining for 3 h at 550 °C at 20 °C min^{-1} under static air.

Preparation of Fe-TS-1

FeTS-1 was prepared using the CVI method as described in the case of FeZSM-5.

Solid state ion exchange (SSIE) procedure involves mixing and grinding the metal precursor and zeolite using a mortar and pestle for 30 min before calcining the dry mixture for 3 h at 550 °C at 20 °C min^{-1}.

Preparation of silicalite-1 (mole ratio template/Si = 1)

Silicalite-1 (SIL-1) was prepared according to Tarramasso *et al.*[27] Tetraethyl orthosilicate (20.48 g, 98.8 mmol) was added dropwise to tetrapropylammonium hydroxide (40 wt. % in H_2O, 25.4 g, corresponding to 10.16 g TPAOH, 49.9 mmol) while stirring vigorously. The resulting gel was stirred for 5 h at 60 °C. Then the gel was transferred to a Teflon-lined stainless steel autoclave and heated in an iso-thermal oven (175 °C, 48 h). The sample was later recovered by centrifugation, washed with deionised water (1 L) and air-dried (110 °C, 16 h). The dried silicalite was calcined (550 °C, 24 h, 1 °C min^{-1}) in flowing air in order to remove the residual organic template.

Preparation of Fe-silicalite-1 (SiO_2/Fe_2O_3 mole ratio = between 130 to 500)

Fe-Silicalite-1 (Fe-SIL-1) was prepared according to Prikhod'ko *et al.*[28] The procedure for a sample with SiO_2/Fe_2O_3 ratio = 260 is exemplified as follows.

Tetra-propylammonium hydroxide (40 wt. % in H_2O, 15 g, corresponding to 6.0 g TPAOH, 30.8 mmol) was stirred vigorously (25 °C, 1 h), and to this solution tetraethyl orthosilicate (20.48 g, 98.8 mmol) was added dropwise. The clear gel obtained was subsequently stirred (60 °C, 3 h). At this time, a 10 mL aqueous solution of $Fe(NO_3)_3.9H_2O$ (0.294 g, 0.76 mmol) and oxalic acid (0.304 g, 2.50 mmol) was added dropwise to obtain a homogeneous, ferrisilicate gel with the following composition;

SiO_2: Fe_2O_3: $H_2C_2O_4$: TPAOH

1 : 0.00385 : 0.013 : 0.312

The resulting gel was subsequently crystallised in a Teflon-lined stainless steel autoclave (175 °C, 120 h). The as-synthesised materials were later recovered by centrifugation, washed with deionised water (1 L) and air-dried (110 °C, 16 h). Calcination process was carried out (550 °C, 8 h, 1 °C min^{-1}) in a flow of nitrogen (5 h) and later air (3 h).

Reaction procedures

Methane oxidation reactions were performed in a stainless steel conventional flow setup. The desired amount (typically 0.44 g) of catalyst (20-40 mesh) was placed in a stainless steel tube sandwiched between two quartz wool plugs. In all cases, the feed mixture (flow rate = 55 ml/min, typically GHSV 3600 h^{-1}) contained 20% CH_4 + 2% N_2O with Ar balance at atmospheric pressure and controlled by mass flow controllers (Bronkhorst UK Ltd) and the reaction temperature was typically 300 °C unless stated otherwise.

Methanol control experiment

MeOH was introduced by flowing a N_2O and Ar mixture through a MeOH-containing Dreschel bottle cooled to ca. 7 °C ± 1°C. In all cases, the fed mixture (flow rate = 55 ml/min) contained 1.2 % MeOH + 2 % N_2O with Ar balance at atmospheric pressure and the reaction temperature set at 300 °C.

Analytical methods

All products in the reaction outlet were analysed with online gas chromatography (GC) at 30 min intervals by Agilent 7890B GC equipped with a methaniser. CH_4, CO, CO_2, ethene, ethane were detected by flame ionisation detector (FID) using a Hayesep packed column. MeOH and DME and other aromatic species were detected by FID with a capillary column. N_2O and N_2 were detected by a thermal conductivity detector (TCD). Products were quantified against a calibration curve constructed from a known amount of the product premixed in house or from commercial standards (BOC).

CH_4 and N_2O conversion was calculated as follows:

$$\mathrm{CH_4\ conversion\ (\%)} = \frac{\mathrm{CH_4}_{in} - \mathrm{CH_4}_{out}}{\mathrm{CH_4}_{in}} \times 100$$

where, $CH_{4\ in}$ and $CH_{4\ out}$ represent the molar fraction of CH_4 at the inlet and outlet, respectively.

$$\mathrm{N_2O\ conversion\ (\%)} = \frac{\mathrm{N_2O_{in}} - \mathrm{N_2O_{out}}}{\mathrm{N_2O_{in}}} \times 100$$

Where, N_2O_{in} and N_2O_{out} represent the molar fraction of N_2O at the inlet and outlet, respectively.

The selectivity for product i (S_i) was calculated as follows, coke assumed to be the remainder:

$$S_i\ (\%)\ = \frac{\text{amount of product (i) produced (mol carbon)}}{\text{CH}_4\ \text{converted (mol of carbon)}}\ \text{x}\ 100$$

Catalyst characterisation

Powder X-ray diffraction (XRD)

XRD was performed on an X'PertPRO PANalytical instrument. A Cu Kα (1.54 Å) radiation source with a nickel filter, calibrated against a Si standard was used. Wide angle measurements were taken in the range of 2θ = 10 – 80°. Approximately 0.3 g of sample was required for each experiment.

UV-vis spectroscopy

UV-Vis analysis was performed on an Agilent Cary 4000 UV-vis spectrophotometer with diffuse reflectance set up. Samples were scanned between 200 – 800 nm at a scan rate at 400 nm min^{-1}.

Ammonia TPD

Temperature-programmed desorption (TPD) of ammonia for the zeolites was carried out in a conventional flow apparatus (Chembet TPR/TPD Chemisorption analyser, Micromeritics Inc.). Sample (0.05 g) was loaded in a U-type tube and sandwiched between quartz wool. The samples were pretreated at 550 °C with a He flow of 145 mL min^{-1} for 1 h to remove residual water and was allowed to cool to room temperature. Ammonia adsorption was carried out by flowing 5% NH_3 in argon to the sample tube for 15 min. The physisorbed ammonia and excess in the sample tube was removed by heat treating the sample tube to 100 °C at 15 °C min^{-1} for 1h and the TPD signal for the desorption of chemisorbed ammonia was recorded from 100 to 900 °C at 10 °C min^{-1} with a thermal conductivity detector (TCD).

Pyridine DRIFTS

Samples were pretreated prior to acquisition by heating the sample in a Harrick Praying Mantis *in situ* cell to 550 °C (20 °C min^{-1}) under flowing nitrogen for 1 h to remove residual water. After the heat treatment, the sample was left to cool down to room temperature before pyridine was introduced to the cell for 5 min. The excess pyridine in the cell was removed by vacuum (10^{-3} mbar) for 5 min and IR spectra were recorded at different temperatures in the range of 30−600 °C under continuous vacuum. The scan was taken 5 min after reaching each of the desired set temperatures.

For *in situ* heat treatments a Harrick Automatic Temperature Controller was used in heating the sample cell according to a predefined (20 °C min^{-1}) heating program. Gas flows were passed through the sample, with flow rates (60 mL min^{-1}) controlled by a Brooks MFC. IR spectra were collected on a Bruker Tensor 27 spectrometer (4000 cm^{-1} - 500 cm^{-1}, 4 cm^{-1} frequency, 64 scans) fitted with a liquid N_2 - cooled Mercury Cadmium Telluride (MCT) detector. The samples were placed within a Praying Mantis high temperature diffuse reflection chamber (HVC-DRP-4) *in situ* cell fitted with zinc selenide windows. Background scans were recorded using dry KBr.

Results and discussion

To investigate the influence of both Fe and Al on the reaction of CH_4 with N_2O, several catalysts were prepared based on the MFI zeolite structure (Table 1). The Fe-doped MFI zeolites have been successful in producing methanol from methane under static[26] or continuous operation.[12] The Fe-MFI catalysts were compared to their corresponding parent zeolites (Table 1, Figs S1-4) over 2 h. The parent SIL-1 and TS-1 zeolites were inactive for methane conversion; however, the low conversion observed over H-ZSM-5 can be attributed to metal impurities introduced during synthesis, such as Fe. This impurity can be present in the 100s ppm and despite being located in framework positions it can activate C-H bonds in the presence of H_2O_2.[15]

The addition of Fe to the parent MFI zeolites clearly illustrates that the reaction environment has a significant impact on the activation of methane. In the case of Fe-SIL-1, the Fe was introduced at the synthesis stage and 0.5 % loading is a compromise to obtain Fe containing samples with an MFI structure. For the Fe-ZSM-5 and Fe-TS-1 samples, the Fe was introduced post-synthesis *via* CVI. In each case we consider that the Fe speciation and location within the MFI structure to be different and will assist in catalyst optimisation. In both the Fe-SIL-1 and Fe-TS-1 only a minor degree of methane and N_2O conversion was recorded. Indeed the activation of N_2O is a key marker to indicate the likely presence of either Fe^{4+}=O or $Fe^{3+}O^{2-}Fe^{3+}$ sites, which are considered as part of the active methane oxidation site.[16] TS-1 is comprised of TiO_4 and SiO_4 tetrahedral units, the absence of Al in TS-1 means there are no Brønsted acid sites only Lewis acid sites. Table 1 illustrates that the TS-1 based materials are inactive for methane oxidation. Therefore, the combination of Fe and framework Al in the Fe-ZSM-5 catalyst can activate methane, although the selectivity to methanol was found to be low. Furthermore, the low mass balance with ca. 63 % selectivity to coke strongly suggests that efficient desorption of reaction products is crucial in this reaction. Diluting the methane feed-stream with water has been used to efficiently desorb methanol from the catalyst[12] and potentially react directly with adsorbed $*CH_3$.[29] Our results support this, as without water CO_x dominates the reactor effluent and the catalysts coke rapidly (Fig. S2).

The results from reactions over the metal-free SIL-1 and Fe-SIL-1 catalysts suggest that Fe has the potential to activate C-H bonds (Table 1). However, the Fe was introduced in the

hydrothermal preparation and is likely to be located in the framework. Introducing iron post-synthesis was investigated to assess if the location of the Fe species would facilitate improved C-H activation without Al present. Using SSIE or CVI approaches should not produce framework Fe species as the SiO_4 tetrahedral units are considered stable and will not permit metal ion exchange. The methane oxidation results illustrated in Table S1 indicate that the Fe-SIL-1 catalysts prepared by either CVI or SSIE are completely inactive. To understand this, UV/Vis spectra of these catalysts were recorded to positively identify the Fe co-ordination environment (Fig. S6). Both the Fe-SIL-1 samples prepared by CVI and SSIE possess a strong and broad absorbance stretch between 310 to 600 nm which suggests that iron oxide clusters are dominant. A weak absorbance at 250 nm potentially corresponds to extra-framework Fe species[30, 31], which is considered part of the active site,[16] however, this proved inactive in the case of the Fe-SIL-1 samples prepared by CVI and SSIE.

The location and likely co-ordination environment of the Fe in both the as-prepared and calcined samples of the 0.5 % Fe-SIL-1 sample was also investigated with UV/Vis spectroscopy (Fig. 1). The distribution of the type of Fe species formed can be revealed from the UV/Vis spectra. For uncalcined Fe-SIL-1, two major bands (210 and 240 nm) were observed, which correspond to the $t_1 \rightarrow t_2$ and $t_1 \rightarrow e$ transitions of the FeO_4 tetrahedra respectively, suggesting the Fe species occupy lattice positions[32, 33]. The sample was then treated at different temperatures, both under flowing air or steam as Fe can migrate out of the MFI framework to occupy positions that are considered to be more catalytically active as with Fe-ZSM-5.[34] In the case of the Fe-SIL-1 samples calcined at 550 °C, the band at 210 nm has decreased indicating a modest migration of Fe away from lattice positions. The modest increase in absorbance from 240 to 300 nm suggests a minor level of migration of tetrahedral framework Fe to extra-framework positions. After steaming the parent sample, the absorbance decreased. Following treatment at 875 °C under both air and steam analysis of the spectra indicates a larger degree of extra-framework Fe present and can be linked to catalytic activity.[35] Analysis of the Fe-SIL-1 samples indicated that the surface was largely free from iron oxide clusters which are characteristic of higher wavelength absorption.

The Fe-SIL-1 samples were tested for methane oxidation in order to understand if the location of the Fe in the catalyst could improve C-H activation (Table 2). The conversion of methane over the sample steamed at 550 °C was comparable to the calcined sample (ca. 0.2 %). This

result indicates that the presence of Fe can potentially activate C-H bonds in the same fashion as H-ZSM-5 with its Fe impurities. Although, the uncalcined Fe-SIL-1 sample possesses framework Fe and is inactive, the pores are likely to be inaccessible due to retention of the TPAOH template. Following higher temperature treatment under air or steam, the activity of the catalyst samples decreased, despite possessing extra-framework Fe. In this case the selectivity to methanol increased, however, as the methane conversion is not equivalent to those treated at lower temperatures it is difficult compare directly. The active site is considered to be an extra-framework mono- or di-Fe species coordinated to a framework Al.[15, 17] According to the UV/Vis spectra (Fig. 1) and the methane oxidation results of the Fe-SIL-1 samples treated at 875 °C, the extra-framework Fe present is unable to activate N_2O (Table 2) compared to the case over Fe-ZSM-5 (Table 1.). Therefore, we consider that the Fe coordination environment is crucial to afford efficient reactivity with N_2O.

High temperature treatment of zeolites can cause a loss of Brønsted acid sites through migration of framework Al.[36] Therefore, we investigated different heat-treatments for the 2 wt.% Fe-ZSM-5 to disrupt the active site and subsequently observe the effect on C-H activation. The sample was treated under static air or dilute, flowing hydrogen over a range of temperatures from 550 to 950 °C and the recovered samples were tested for methane oxidation using N_2O as the oxidant (Table 3). The oxidising or reducing environments of this catalyst pre-treatment step will have different water content, which was found to be crucial to dealumination.[36] The samples treated at 550 and 750 °C under both air and hydrogen resulted in comparable methane conversions of ca. 2 %. In all cases the mass balance was low, as observed with the 2 wt.% Fe-ZSM-5 calcined at 550 °C. However, after heat treatment under air at 950 °C, the catalyst appears to undergo an irreversible change and the result is a significant loss in activity. Both the conversion of methane and N_2O are greatly affected, however, the space-time-yield of methanol was calculated to be ca. 19 µmol g_{cat}^{-1} h^{-1}. Conversely, over 2 wt.% Fe-ZSM-5 calcined at 550 °C the STY_{MeOH} was found to be significantly lower at ca. 6 µmol g_{cat}^{-1} h^{-1}. Testing of the sample following treatment at the same temperature under the dilute hydrogen atmosphere suggests it did not undergo such a change. Powder XRD of the samples (Fig. S5) indicates that the MFI structure is retained at the higher temperatures, consistent with previous reports.[36] The testing results detailed in Table 3 suggest that the active site is stable to 750 °C and the presence of ethene in the

reactor effluent indicates the surface Brønsted acidity is not compromised. In contrast the presence of DME in the effluent over 2 wt.% Fe-ZSM-5 calcined at 950 °C in air suggests that the high temperature and moisture present has affected the Brønsted acidity.

Pyridine desorption experiments were carried out using DRIFTS to monitor the changes in both Lewis and Brønsted acidity as a function of temperature, shown in Figure 2. The temperature of desorption, or loss of adsorption band, indicates the strength of the different acid sites. The pyridine absorbance at 1450 cm^{-1} corresponds to the pyridine adsorption on a Lewis acid sites, while the Brønsted acid sites can be observed by the band at 1540 cm^{-1} which corresponds to the C-C bond vibration of the pyridinium ion. The absorbance at 1490 cm^{-1} indicates the pyridine interaction of both type of acid sites.[37] Comparison of the peaks present over the samples studied at room temperature indicate that the heat treatment at 950 °C under air has clearly increased the number of Lewis acid sites as the band at 1450 cm^{-1} has significantly increased. We consider this to be due the migration of aluminium forming greater Lewis acid sites within the pore channels.[23] However, these may be of lower strength as pyridine is quickly lost from this site, as the corresponding reduction in the band at 1440 cm^{-1} over the measurements taken below 100 °C suggests. As the temperature of this sample is heated the peak profile reduces until no pyridine remains adsorbed at 400 °C. In contrast, pyridine remains adsorbed until 500 °C on the Fe-ZSM5 samples heated at 550, 750 and treated under H_2 at 950 °C. Despite retaining a degree of surface acidity the Fe-ZSM-5 catalysts calcined under air at 950 °C was essentially inactive (Table 3.).

We consider that the Fe coordination environment is crucial with respect to the activation of C-H bonds. The heat treatment under air at 950 °C has disrupted this environment *via* migration of Al species as reported previously[36] and efficient N_2O decomposition cannot occur (Table 3). In Figure 2f, the area of each absorbance band, normalised against the zeolite framework overtones at 2010 cm^{-1}, is presented. This method was previously reported when comparing the acidity of ZSM-5 catalysts after high temperature calcinations[36]. Figure 2f is a comparison of the pyridine DRIFTS data at 300 °C and clearly shows that the addition of Fe decreases the Brønsted acidity of the catalyst. This is expected as the Fe is considered to co-ordinate to the framework Al, thereby disrupting the Brønsted acid site. Further heat treatment at 750 and 950 °C lead to a further decrease in Brønsted acidity, consistent with the de-alumination of the zeolite. Interestingly, the addition of Fe to the H-ZSM-5 increased

the size of the absorbance band associated with Lewis acidity, which did not appear to change significantly after calcination at 750 °C, but significantly decreased after calcination at 950 °C. It can therefore be concluded that the high temperature calcinations significantly decreased the number Brønsted acid sites.

The pyridine desorption experiments were complemented by NH_3-TPD under similar conditions to investigate the relative acid strength of the series of catalysts under study (Fig. 3). There are two characteristic signals that are often observed in the NH_3-TPD spectra using MFI zeolites. The desorption features are located at 260 °C and 450-550 °C, which represent the weak (low temperature desorption, LT) and strong acid sites (high temperature desorption, HT) respectively. The strong acid sites (HT) are generally used to evaluate the acid strength of the catalysts due to the weak acid sites representing the desorption from non-acidic sites or physisorbed NH_3.[38] The area of the HT desorption feature indicates the concentration of the acid sites and the temperature at which the HT peak maximum occurs indicate the overall acid strength of the sample.[39] The addition of Fe to the ZSM-5 framework modestly altered the strength of the strong acid sites (HT). In contrast, calcination at 750 and 950 °C shifted the NH_3 desorption for the strong acid sites from 450 °C to 520 and 580 °C respectively. In addition, the overall quantity of NH_3 adsorbed is lower with these materials calcined at higher temperatures. Furthermore, the decrease of overall acidity observed with the sample calcined at 950 °C corresponded to an increase in the acid strength. This suggests that only the Brønsted acid sites have increased in strength following heat treatment, due to the observed increased adsorption of pyridine at low temperatures on Lewis acid sites. This result highlights the importance of the acid sites and their concentration for the methane activation through the formation of the active α-oxygen species. The increase of acid strength and density of Lewis acid sites has resulted in significantly reduced activity, which further suggests that Fe must be coordinated to framework Al for efficient formation of active oxygen sites.

The active Fe site has been reported to be co-ordinated to framework Al[40] and therefore the maximum number of active Fe sites is proportional to the Al content. A series of Fe-ZSM-5 catalysts were prepared that had the same Fe:Al ratio from parent H-ZSM-5 catalysts with varying SiO_2:Al_2O_3 ratios. The catalytic activity is presented in Table 4. The Fe:Al ratio of 0.47 was applied to ZSM-5 catalysts with SiO_2:AlO_3 ratios of 23, 30, 50 and 280, and led to Fe

loadings of 2.7 to 0.3 wt.%. Analysis of the Fe environment by UV/Vis was not carried out due to the high Fe loadings present, which easily obscure identifiable features. The methane and N_2O conversion increased with increasing Al loading from 0.5 to 2.5 % and 3.4 to 27.2 %. However, the N_2O TOF as a function of Fe content remained comparable at ca. 3.5 h^{-1} across the samples and we assume the Fe environment is comparable across the samples. The selectivity to coke can be seen to reduce according to the methane conversion and Al content. Furthermore, this suggests that the acidity of the MFI surface plays a significant role in the retention of methanol and subsequent coke formation. However, the reactions were not carried out at iso-conversion and comparison such as this is not ideal.

The role of acidity and Fe location was further investigated with respect to the low methanol selectivity and low mass balances observed over catalysts such as the 2 wt.% Fe-ZSM-5 (calcined at 550 °C). Control experiments were carried out using methanol, considered to be a primary product, diluted in an Ar stream containing N_2O. Methanol is known to react efficiently over ZSM-5 catalysts to form primarily DME and olefins in a process commonly referred to as methanol-to-olefins (MTO).[41] Methanol undergoes the hydrogen pool mechanism to form various hydrocarbons in the zeolite pores.[42] Wang *et al.* reported that in the case of H-ZSM-5, methyl substituted 5-6 membered ring reactive carbenium intermediates such as pentamethylbenzenium ($PentaMB^+$), di/tri-methylcyclopentenyl cation (diMCP+, triMCP+) can be generated.[43] Those cyclic organic species confined in zeolite cages/intersection space could act as a co-catalyst for ethene formation *via* side chain elimination from MCP^+.[44] In this study we were able to detect trace amount of aromatic species including methyl benzene, toluene and xylene which may explain the origin of ethene and coke generated from a competing reaction path.

Dilute methanol vapour was passed over the MFI-based catalysts with N_2O present in order understand the stability and reactivity of the target product under reaction conditions. The catalysts used were the Fe-free H-ZSM-5, SIL-1, TS-1 and their Fe containing analogues. The catalyst mass was adjusted to ensure comparable methanol conversions of ca. 15 % at 300 °C while maintaining a GHSV of 3600 h^{-1} through dilution with SiC (Table 5 and time-on-line data for the active catalysts in Fig. S8-12). Interestingly, methanol conversion was observed in H-ZSM-5 and all the Fe-containing catalysts and the primary product in each case was DME. The results over the SIL-1 and TS-1 materials strongly indicate that Brønsted acidity is required to

complete the formation of DME as previously reported.[44, 45] Over H-ZSM-5 the selectivity to DME was ca. 44 % and for ethene ca. 16 % at 65 minutes, which is consistent with previous reports.[41] The time-on-line data clearly indicates that the increased selectivity to C_{2+} products results in the low mass balance observed through the subsequent formation of retained organics. The time-on-line data suggest that the catalyst is relatively stable over the 2 h of reaction (Fig. S8). In contrast, the yield of DME, over the 2 wt.% Fe-ZSM-5 (550 °C) catalyst decreased rapidly over the 2 h reaction period and an increase of ethene was noted. Although, ethene was formed over the 2 wt.% Fe-ZSM-5 (950 °C) catalyst, the STY was low at ca. 4 µmol g^{-1} h^{-1} after 125 min time-on-line. Over the 0.5 wt.% Fe-SIL-1 catalyst steamed at 875 °C the conversion of methanol to DME proceeds readily despite the absence of Al and the extra-framework Fe. This is exemplified by the high DME selectivity of 95 % achieved over the Fe-TS-1 catalyst.

These results imply that the presence of acidity related to Al is not necessarily required to support the methanol condensation reaction to form DME. However, the strength of the acid sites illustrated in Figure 2 clearly relate to the formation of coke at 300 °C (Table 5) and subsequent reduction in mass balance observed. Furthermore, these results support the low methanol selectivity observed in the methane oxidation reactions where water is not present in the feed (Table 1). The challenge of selective methane oxidation is exemplified here as methanol is significantly more reactive than methane over the acidic MFI catalysts. Indeed, over MFI catalysts with moderate to high acidity such as 2 wt.% Fe-ZSM-5 (550 °C) any DME produced at the low methane conversions achieved, appears to convert rapidly to other products such as ethene, unlike over 2 wt.% Fe-ZSM-5 (950 °C) catalyst (Table 5). An additional consideration is the relatively high concentration of methanol in the feed stream that may operate in a comparable manner to using methane diluted with water[21, 46]. That is, the product is displaced rapidly from the active site with water and hence the selectivity to methanol from methane is high, such as DME from methanol in these experiments. Furthermore, ethene and coke are only formed over catalysts with Al present, via the Brønsted acid sites under these reaction conditions. The implication is that framework Al sites free of Fe are able to convert methanol efficiently. Therefore, tailoring the acidity and Fe loading of the catalyst can significantly improve methanol yields.

Conclusions

The continuous oxidation of methane by N_2O was investigated with a series of MFI-based zeolites. The parent zeolites; SIL-1, TS-1 and H-ZSM-5 were tested and the results suggest that the activation of methane occurs only in the case of H-ZSM-5. However, the presence of metal impurities is likely to be the origin of the minor activity observed. The addition of Fe to the parent materials enhanced the methane activation in the case of the ZSM-5, although the catalyst exhibited a poor carbon mass balance as the reaction proceeded. The origin of the low mass balance and increased catalyst fouling was investigated through exploration of the catalyst acidity and location and speciation of Fe. Where extra-framework Fe was prepared through heat treatments on Fe-SIL-1, C-H activation did not occur. Methanol control experiments indicated that methanol is unstable over catalysts with high Brønsted acidity such as H-ZSM-5 and those containing Fe such as Fe-SIL-1 and Fe-TS-1. However, the formation of C_{2+} and aromatic species was only observed in the case of the ZSM-5 catalysts and this supports the observed low methanol selectivity and mass balances observed in the methane oxidation reaction. The results suggest that through manipulation of catalyst acidity and Fe concentration, improvements in methanol selectivity can be achieved where desorption of the primary product is facile. This study also demonstrates that for selective methane oxidation with N_2O, extra-framework Fe species co-ordinated to framework Al are required. However, Brønsted acid sites located on Fe-free Al lead to the transformation of methanol into coke.

Acknowledgments

The authors wish to thank ExxonMobil for financial support.

References

1. A. I. Olivos-Suarez, A. Szecsenyi, E. J. M. Hensen, J. Ruiz-Martinez, E. A. Pidko and J. Gascon, *ACS Catal.*, 2016, **6**, 2965-2981.
2. K. Aasberg-Petersen, I. Dybkjaer, C. V. Ovesen, N. C. Schjodt, J. Sehested and S. G. Thomsen, *J. NAT. GAS SCI. ENG.*, 2011, **3**, 423-459.
3. N. D. Parkyns, C. I. Warburton and J. D. Wilson, *Catal. Today*, 1993, **18**, 385-442.
4. B. A. Arndtsen, R. G. Bergman, T. A. Mobley and T. H. Peterson, *Acc. Chem. Res.*, 1995, **28**, 154-162.
5. J. A. Labinger, *J. Mol. Catal. A Chem.,* 2004, **220**, 27-35.
6. D. F. McMillen and D. M. Golden, *Annu. Rev. Phys. Chem.*, 1982, **33**, 493-532.
7. N. Dietl, M. Schlangen and H. Schwarz, *ANGEW. CHEM. INT. EDIT.* , 2012, **51**, 5544-5555.
8. G. I. Panov, A. K. Uriarte, M. A. Rodkin and V. I. Sobolev, *Catal. Today*, 1998, **41**, 365-385.
9. E. V. Starokon, M. V. Parfenov, S. S. Arzumanov, L. V. Pirutko, A. G. Stepanov and G. I. Panov, *J. Catal.*, 2013, **300**, 47-54.
10. E. V. Starokon, M. V. Parfenov, L. V. Pirutko, S. I. Abornev and G. I. Panov, *J. Phy. Chem. C* , 2011, **115**, 2155-2161.
11. E. V. Starokon, M. V. Parfenov, S. E. Malykhin and G. I. Panov, *J. Phy. Chem. C* , 2011, **115**, 12554-12559.
12. M. V. Parfenov, E. V. Starokon, L. V. Pirutko and G. I. Panov, *J. Catal.*, 2014, **318**, 14-21.
13. A. Zecchina, M. Rivallan, G. Berlier, C. Lamberti and G. Ricchiardi, *Phys. Chem. Chem. Phys.*, 2007, **9**, 3483-3499.
14. B. E. R. Snyder, P. Vanelderen, M. L. Bols, S. D. Hallaert, L. H. Bottger, L. Ungur, K. Pierloot, R. A. Schoonheydt, B. F. Sels and E. I. Solomon, *Nature*, 2016, **536**, 317-+.
15. C. Hammond, N. Dimitratos, R. L. Jenkins, J. A. Lopez-Sanchez, S. A. Kondrat, M. H. ab Rahim, M. M. Forde, A. Thetford, S. H. Taylor, H. Hagen, E. E. Stangland, J. H. Kang, J. M. Moulijn, D. J. Willock and G. J. Hutchings, *ACS Catal.*, 2013, **3**, 689-699.
16. C. Hammond, M. M. Forde, M. H. Ab Rahim, A. Thetford, Q. He, R. L. Jenkins, N. Dimitratos, J. A. Lopez-Sanchez, N. F. Dummer, D. M. Murphy, A. F. Carley, S. H. Taylor, D. J. Willock, E. E. Stangland, J. Kang, H. Hagen, C. J. Kiely and G. J. Hutchings, *ANGEW. CHEM. INT. EDIT.*, 2012, **51**, 5129-5133.
17. K. A. Dubkov, N. S. Ovanesyan, A. A. Shteinman, E. V. Starokon and G. I. Panov, *J. Catal.*, 2002, **207**, 341-352.
18. A. M. DeGroote and G. F. Froment, *Catal. Today*, 1997, **37**, 309-329.
19. G. K. Boreskov, Springer Berlin Heidelberg, Berlin, Heidelberg, 1982, pp. 39-137.
20. K. Narsimhan, K. Iyoki, K. Dinh and Y. Roman-Leshkov, *ACS Cent. Sci.*, 2016, **2**, 424-429.
21. P. Tomkins, A. Mansouri, S. E. Bozbag, F. Krumeich, M. B. Park, E. M. C. Alayon, M. Ranocchiari and J. A. van Bokhoven, *ANGEW. CHEM. INT. EDIT.*, 2016, **55**, 5467-5471.
22. G. Sastre and A. Corma, *J. Mol. Catal. A Chem.*, 2009, **305**, 3-7.
23. E. G. Derouane, J. C. Vedrine, R. R. Pinto, P. M. Borges, L. Costa, M. Lemos, F. Lemos and F. R. Ribeiro, *Cat. Rev. - Sci. Eng.*, 2013, **55**, 454-515.
24. C. Mirodatos and D. Barthomeuf, *J. Chem. Soc., Chem. Commun.*, 1981, 39-40.

25. M. Niwa, S. Sota and N. Katada, *Catal. Today*, 2012, **185**, 17-24.
26. W. F. Hoelderich, *Appl. Catal., A*, 2000, **194**, 487-496.
27. *United States Pat.,* 1982.
28. R. V. Prikhod'ko, I. M. Astrelin, M. V. Sychev and E. J. M. Hensen, *Russ. J. Appl. Chem.,* 2006, **79**, 1115-1121.
29. M. He, J. Zhang, X. L. Sun, B. H. Chen and Y. G. Wang, *J. Phy.l Chem. C*, 2016, **120**, 27422-27429.
30. E. J. M. Hensen, Q. Zhu, R. A. J. Janssen, P. Magusin, P. J. Kooyman and R. A. van Santen, *J. Catal.*, 2005, **233**, 123-135.
31. M. Schwidder, W. Grunert, U. Bentrup and A. Bruckner, *J. Catal.*, 2006, **239**, 173-186.
32. S. Bordiga, R. Buzzoni, F. Geobaldo, C. Lamberti, E. Giamello, A. Zecchina, G. Leofanti, G. Petrini, G. Tozzola and G. Vlaic, *J. Catal.*, 1996, **158**, 486-501.
33. E. J. M. Hensen, Q. Zhu, M. M. R. M. Hendrix, A. R. Overweg, P. J. Kooyman, M. V. Sychev and R. A. van Santen, *J. Catal.*, 2004, **221**, 560-574.
34. G. N. Li, E. A. Pidko, I. A. W. Filot, R. A. van Santen, C. Li and E. J. M. Hensen, *J. Catal.*, 2013, **308**, 386-397.
35. J. Perez-Ramirez, *J. Catal.*, 2004, **227**, 512-522.
36. T. C. Hoff, R. Thilakaratne, D. W. Gardner, R. C. Brown and J. P. Tessonnier, *J. Phy. Chem. C*, 2016, **120**, 20103-20113.
37. F. Jin and Y. D. Li, *Catal. Today*, 2009, **145**, 101-107.
38. Q. Zhao, W. H. Chen, S. J. Huang, Y. C. Wu, H. K. Lee and S. B. Liu, *J. Phy. Chem. B*, 2002, **106**, 4462-4469.
39. J. H. C. van Hooff and J. W. Roelofsen, *Stud. Surf. Sci. Catal.*, 1991, **58**, 241-283.
40. P. Pramatha and K. D. Prabir, in *Handbook of Zeolite Science and Technology*, CRC Press, 2003.
41. M. Bjorgen, S. Svelle, F. Joensen, J. Nerlov, S. Kolboe, F. Bonino, L. Palumbo, S. Bordiga and U. Olsbye, *J. Catal.,* 2007, **249**, 195-207.
42. I. M. Dahl and S. Kolboe, *J. Catal.*, 1994, **149**, 458-464.
43. C. Wang, X. F. Yi, J. Xu, G. D. Qi, P. Gao, W. Y. Wang, Y. Y. Chu, Q. Wang, N. D. Feng, X. L. Liu, A. M. Zheng and F. Deng, *CHEM-EUR J.*, 2015, **21**, 12061-12068.
44. P. Tian, Y. X. Wei, M. Ye and Z. M. Liu, *ACS Catal*, 2015, **5**, 1922-1938.
45. J. Z. Li, Y. Qi, L. Xu, G. Y. Liu, S. H. Meng, B. Li, M. Z. Li and Z. M. Liu, *Cat. Commun.*, 2008, **9**, 2515-2519.
46. V. L. Sushkevich, D. Palagin, M. Ranocchiari and J. A. van Bokhoven, *Science*, 2017, **356**, 523-+.

Tables and Figures

Table 1. Comparison of MFI catalysts for methane oxidation with N_2O.

Catalyst	Conversion[a] (%)		Selectivity[a] (%)						STY_{MeOH}[b] (μmol g_{cat}^{-1} h^{-1})
	N_2O	CH_4	MeOH	CO	CO_2	C_2H_4	DME	Coke	
Blank tube	-	-	-	-	-	-	-	-	-
SIL-1	-	-	-	-	-	-	-	-	-
HZSM-5 (30)	2.3	0.15	0.6	56.3	14.4	8.8	-	19.9	0.55
TS-1	-	-	-	-	-	-	-	-	-
0.5 %Fe-SIL-1	2.0	0.19	0.3	77.5	22.0	-	-	0.2	0.28
2% Fe-ZSM-5	21.5	1.8	1.1	24.3	9.5	3.5	-	62.6	6.4
2% Fe-TS-1	0.4	<0.05	-	17.7	82.3	-	-	<0.5	-

[a] Values after 1 h on-stream; [b] STY_{MeOH}: space time yield of methanol; Reaction conditions: 0.44 g catalyst; Pellet Mesh size = 600 μm ; V = 0.9 ml ; 300 °C; 2 h; Feed mixture: 20%CH_4 + 2% N_2O with Ar balance; Flow rate = 55 ml min^{-1}; P(total) = 1 atm; GHSV= 3600 h^{-1}.

Table 2. Methane oxidation over 0.5 wt.% Fe-SIL-1 materials prepared by different heat treatments

Catalyst	Conversion[a] (%)		Selectivity[a] (%)						STY_{MeOH}[b] (μmol g_{cat}^{-1} h^{-1})
	N_2O	CH_4	MeOH	CO	CO_2	C_2H_4	DME	Coke	
SIL-1 (Metal-free)	-	-	-	-	-	-	-	-	-
Fe-SIL-1 (uncalcined)	-	<0.05	-	-	1.2	-	-	-	-
Fe-SIL-1 (calcined 550 °C)	2.0	0.19	0.3	22.0	77.5	-	-	-	0.28
Fe-SIL-1 (steamed 550 °C)	2.8	0.25	0.21	74.9	22.3	-	-	-	0.27
Fe-SIL-1 (calcined 875 °C)	1.7	0.19	0.3	73.2	26.5	-	-	-	0.33
Fe-SIL-1 (steamed 875 °C)	1.1	0.08	3.0	70.9	26.1	-	-	-	1.28
Fe-SIL-1 (calcined 875 °C) for 24h	1.5	0.05	2.3	74	23.6	-	-	-	1.1

[a] Values at 1 h; [b] STY_{MeOH}: space time yield of methanol; Reaction conditions: 0.44 g catalyst; Pellet Mesh size = 600 μm; V = 0.9 ml ; 300 °C; 2 h; Feed mixture: 20%CH_4 + 2% N_2O with Ar balance; Flow rate = 55 ml min^{-1}; P(total) = 1 atm; GHSV= 3600 h^{-1}.

Table 3. Methane oxidation over 2 wt.% Fe-ZSM-5 prepared with different calcination conditions.

Calcination temperature (°C) and condition	Conversion[a] (%)		Selectivity[a] (%)						STY_{MeOH}[b] (μmol g_{cat}^{-1} h^{-1})
	N_2O	CH_4	MeOH	CO	CO_2	C_2H_4	DME	Coke	
550 (static air)	21.5	1.8	1.1	24.3	9.5	3.5	-	61.6	6.4
550 (H_2/Ar)	26.0	2.0	0.7	13.4	8.2	3.8	-	73.9	7.1
750 (static air)	20.7	1.9	1.4	26.4	9.3	2.0	-	60.9	12.8
750 (H_2/Ar)	30.6	2.2	0.8	16.1	9.8	2.3	-	71	9.0
950 (static air)	4.4	0.2	13.7	76.8	4.9	-	4.6	-	18.7
950 (H_2/Ar)	29.5	1.4	1.6	25.1	14.0	4.2	-	55.1	13.6

[a] Values after 1 h on-stream; [b] STY_{MeOH}: space time yield of methanol; Reaction conditions: 0.44 g catalyst; Pellet Mesh size = 600 μm ; V = 0.9 ml ; 300 ^{o}C; 2 h; Feed mixture: 20%CH_4 + 2% N_2O with Ar balance; Flow rate = 55 ml min^{-1}; P(total) = 1 atm; GHSV= 3600 h^{-1}.

Table 4. Methane oxidation over Fe-ZSM-5 catalysts (Si:Al of 23 to 280) at 300°C.

Fe content (wt.%) on ZSM-5 {Si:Al}	Conversion[a] (%)		TOF[b]	Selectivity[a] (%)					STY_{MeOH}[c] ($\mu mol\ g_{cat}^{-1}\ h^{-1}$)
	N_2O	CH_4		MeOH	CO	CO_2	C_2H_4	Coke	
2.7 {23}	27.2	2.5	3.1	0.3	10.5	6.4	3.2	79.6	4.9
2.0 {30}	22.5	1.7	3.8	0.8	19.3	8.6	4.4	66.9	6.6
1.2 {50}	11.9	0.9	3.3	0.8	36.0	12.8	1.9	48.5	3.9
0.3 {280}	3.4	0.5	3.8	0.9	38.6	11.9	1.9	46.7	2.4

[a] Values taken from average of 2 h; [b] moles of N_2O converted per moles of Fe present; [c] STY_{MeOH}: space time yield of methanol; Reaction conditions: 0.44 g catalyst; Pellet Mesh size = 600 µm ; V = 0.9 ml; 2 h; Feed mixture: 20% CH_4 + 2% N_2O with Ar balance; Flow rate = 55 ml min^{-1}; P(total) = 1 atm; GHSV= 3600 h^{-}

Table 5. Methanol control experiments over MFI catalysts calcined 550 °C unless otherwise stated.

Catalyst	Catalyst mass (g)	Conversion[a] (%)		Selectivity[a] (%)					Specific Activity [b] (mol g^{-1} h^{-1})
		MeOH	N_2O	DME	CO	CO_2	C_2H_4	Coke	
H-ZSM-5	0.05	14.8	0.5	44.4	0.1	0.06	16.4	39.0	0.266
TS-1	0.4	-	-	-	-	-	-	-	-
SIL-1	0.4	-	-	-	-	-	-	-	-
2% Fe-ZSM5	0.05	16.1	6.5	54.3	0.5	0.2	8.0	37.0	0.290
2% Fe-ZSM5 (calcined 950 °C)	0.05	12.8	1.3	88.1	0.2	0.06	1.6	10.0	0.230
2% Fe-TS1	0.1	17.4	0.7	95.1	1.8	0.14	-	3.0	0.157
0.5% Fe-SIL-1 (steamed 875 °C)	0.4	17.3	1.2	86.6	1.8	0.4	-	11.2	0.039

[a] Values at 65 min; [b] Moles of MeOH converted per g of catalyst per hour; reaction conditions: catalyst mass = varied between 0.05 – 0.4 g and diluted to 1 mL with SiC; GHSV 3600 h^{-1}, Pellet Mesh size = 600 µm; V = 0.9 ml ; 300 ℃; 2 h; Feed mixture: 1.2% MeOH + 2% N_2O with Ar balance; Flow rate = 55 ml min^{-1}; P(total) = 1 atm.

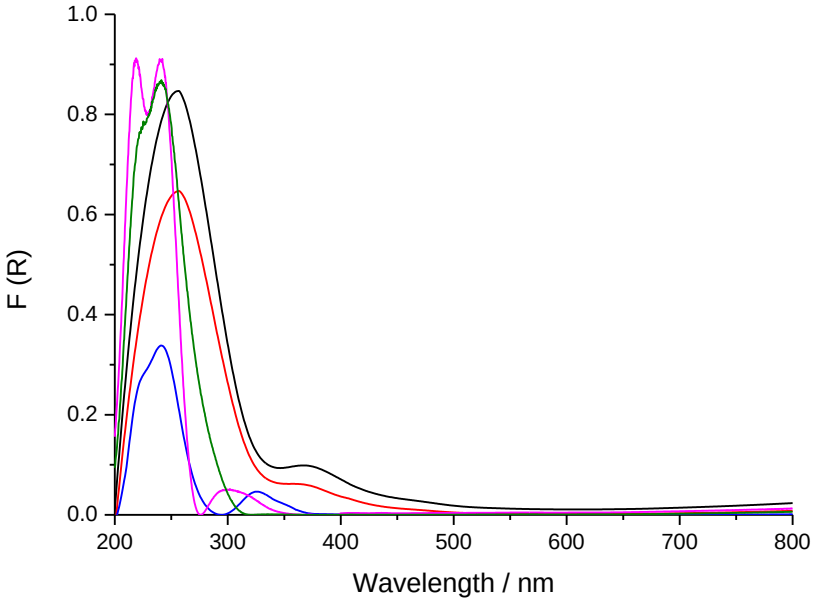

Fig. 1. UV-Vis spectra for the as prepared 0.5 wt.% Fe-SIL-1 sample compared to those following heat treatments under different conditions; uncalcined (magenta), calcined 550 °C (green), steamed 550°C (blue), calcined 875°C (red) and steamed 875°C (black).

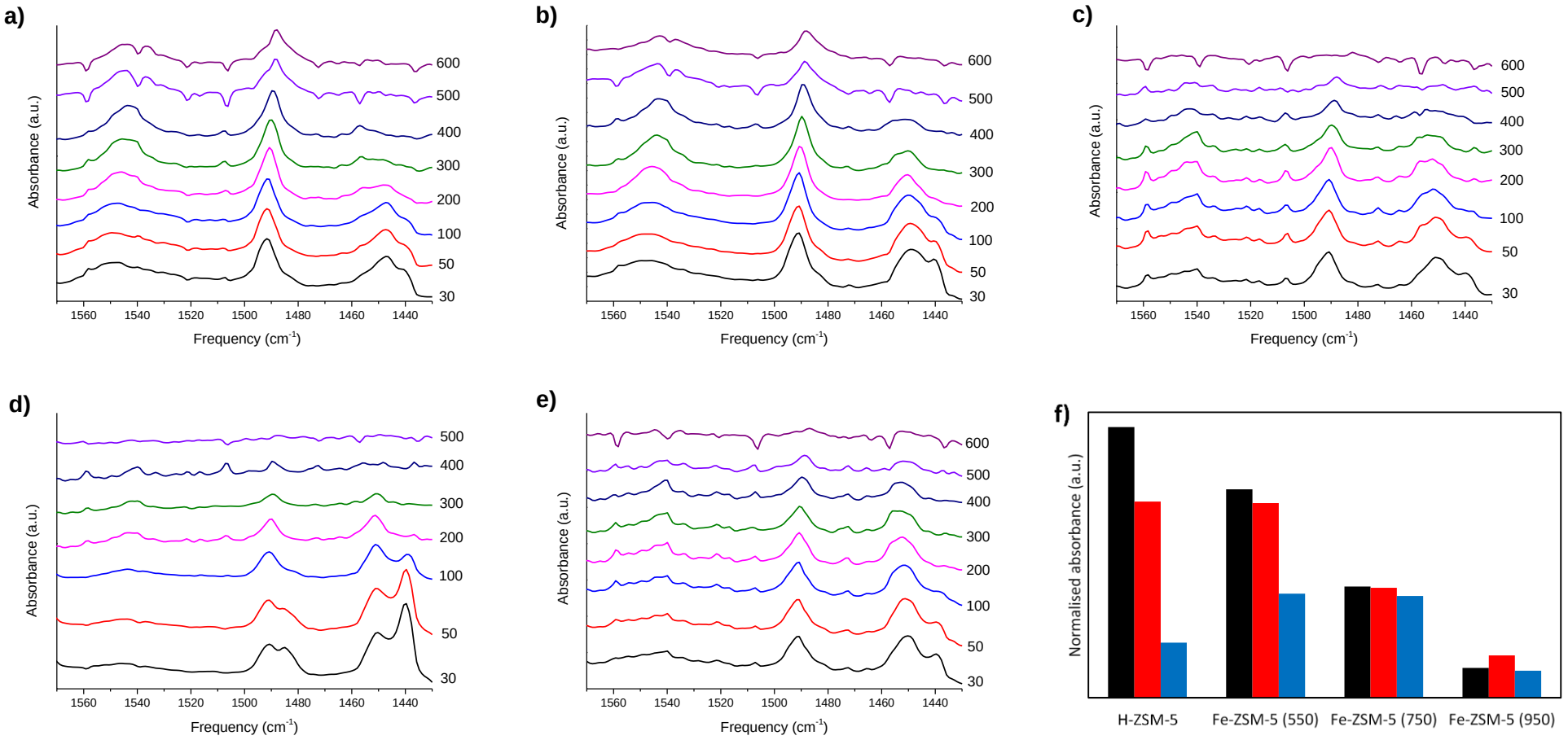

Fig. 2. FTIR spectra of pyridine adsorbed on ZSM-5 materials recorded between 30 - 600 °C; a) H-ZSM-5; and Fe-ZSM-5 calcined at b) 550 °C, c) 750 °C, d) 950 °C under static air and e) calcined at 950 °C under H_2/Ar. f) The absorbance of the Brønsted acid sites (black), Brønsted + Lewis acid sites (red) and Lewis acid sites (blue) of the different ZSM-5 catalysts after different calcination temperatures. The area of the absorbance bands were normalised against the framework overtones at 2010 cm^{-1} at 300 °C.

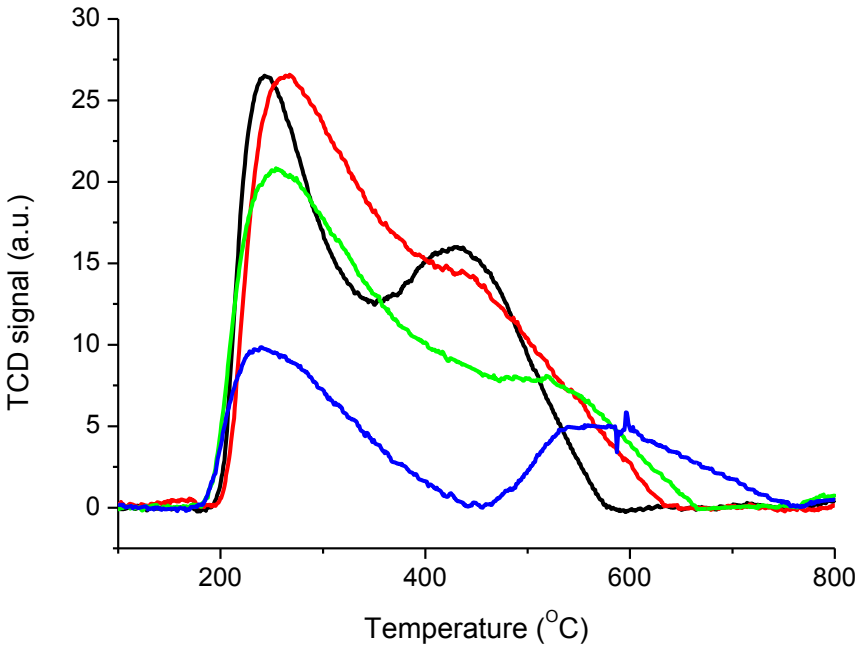

Fig. 3. NH_3 – TPD profile obtained for the ZSM-5 based materials calcined at different temperatures under static air; black line: H-ZSM-5 (550 °C); red line: Fe-ZSM-5 (550 °C); green line: Fe-ZSM-5 (750 °C); blue line: Fe-ZSM-5 (950 °C).